Innovative tools for offshore wind and DC grids

Deliverable 1.3 – Work Package 1
Methodology for reducing the weight and costs of the HV and MV equipment for connecting to AC and DC systems

Website	http://innodc.org/
Grant Agreement number	765585
Due delivery	Month 24: 31 August 2019
Project dates	01/09/2017 – 31/08/2021

Authors	**Names**
ESR1	Peng Yang
ESR4	Davide Pinzan
ESR5	Daniel Westerman Spier
ESR12	Stephen Hardy
ESR14	Motaz Ayiad
Supervisor (KU Leuven)	Hakan Ergun
Supervisor (UPC) WP1 leader	Eduardo Prieto-Araujo

Summary

This document contains a description of the InnoDC project Deliverable 1.3. It details the Methodology employed for reducing the weight and costs of the HV and MV equipment for connecting offshore wind power plants to AC and DC systems.

Contents

1 Introduction

Offshore wind electrical systems are complex networks designed to collect and transmit wind energy to an onshore network for eventual consumption at a load centre. This Deliverable discusses the cost and size reduction of the overall electrical system, from offshore apparatus harvesting the wind energy, to the onshore components which integrate the Offshore Wind Power Plant (OWPP) to the main onshore grid. The analysed equipment consists of platforms, cables, transformers, converters and the accordingly selected insulation, as well as the cyber equipment which is required to acquire data, and to control the overall system for fault and energy management according to weather wind predictions and agreements on real time pricing of the renewable sourced electricity generated and transmitted to the load centers.

1.1 Differences between Onshore and Offshore Wind

Onshore and Offshore Wind Power Plants share many aspects, but for the understanding of cost and weight reduction, hereby discussed, it is fundamental to understand their differences which are explained as follows.

Firstly, given the fact that submarine transmission relies on cables, capacitive effects are much more acute and restrict the maximum transmission distance feasible with High Voltage AC (HVAC) transmission in comparison to "classic" overhead line transmission on land [1]. Secondly, although the installation of submarine cables may be cheaper than land based high voltage cable systems, the cost of building structures, such as offshore substations (OSS) or compensation platforms on water is high compared to land. Offshore substructures are required for both the wind turbines and the OSS. They account for approximately 25% of the total OWPP cost [2]. As such, equipment volume and mass mounted on offshore structures should be minimized.

Finally, the intermittent nature of wind energy must always be considered when choosing equipment. When sizing equipment offshore it is rarely sufficient to size based on peak load alone [3]. Rather, a holistic approach that minimizes the cost of energy production over a plant's lifetime should be adopted. This requires considering quantities such as fixed and variable losses of the entire system, system reliability and Expected Energy Not Served (EENS) from the very earliest development phases [4].

1.2 Methodology

To optimize the cost of the offshore electrical system, a hierarchy of priorities should first be established. For this, a breakdown of the total system costs is useful. On the left most side of Fig. 1 major contributors to OWPP development cost are shown. The transmission system constitutes more than 80% of total expenditure [5] of the grid connection. As such, savings within the HV network have a greater overall impact on total cost and should be prioritized.

The central and right most charts in Fig. 1 breakdown the cost of the electrical network based on transmission technology. In AC systems, over 60% of total cost is caused by the cables and their installation. A further 17% divided among losses and the EENS over the life time of the system as well as required reactive power compensation equipment, heavily impacted by the choice of the HV cables. Contrasting this with a mere 21% for the offshore and onshore transformer stations combined, it is clear that prioritizing cable costs is logical [6].

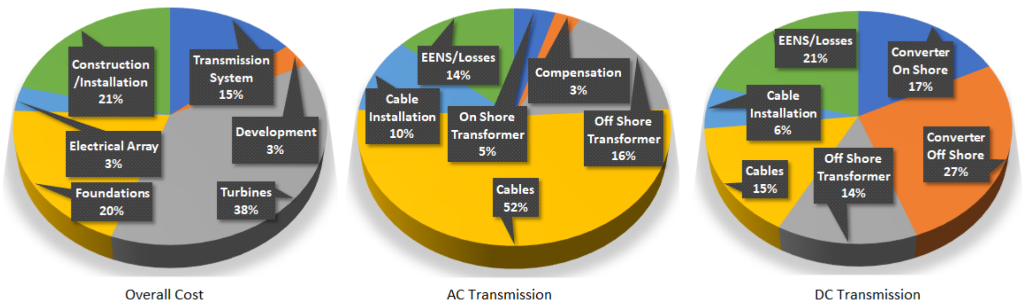

Figure 1: Cost Breakdown of Offshore Wind Power. [5, 6]
AC and DC data are representative of a 300 MW OWPP, 75 km from shore.

In dc systems, a near opposite relationship exists. The onshore and offshore converter stations make up the largest component of the overall cost at 44% with an additional 14% for the offshore transformer feeding the converter [6]. As the onshore converter station does not have the same volume and mass restrictions as its offshore counterpart and the point of grid coupling is generally defined by the existing onshore network, it is the offshore converter station that provides the possibility for highest overall reduction in cost of an HVDC offshore network.

Since the focus of cost reduction for AC and DC systems is not the same, it is important to select the appropriate transmission technology early in the optimization process. Therefore, a solid understanding of which conditions favour one technology over the other is essential. Fig. 2 displays the regions where each technology is most economic over a range of possible power ratings and offshore transmission distances [7]. Mid point compensated AC connections have been shown to increase the viable range of AC connections [8]. Zones shown in black and green are where cost for both technologies is similar and further detailed analysis is required on a per project basis.

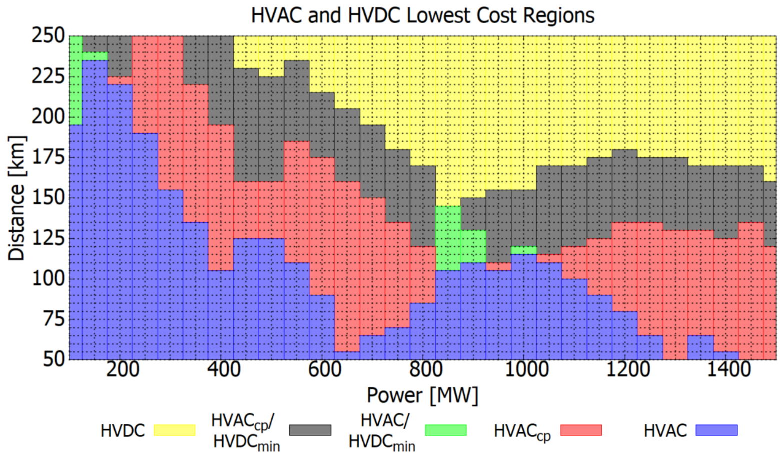

Figure 2: HVDC vs HVAC Transmission Regions [7]

As demonstrated, the selection of the proper technology requires knowledge of both capacity and distance of the offshore connection. Unfortunately, for anything other than single point to point connections of individual OWPPs both transmission distance and capacity are unknowns prior to establishing the connection topology. This means that the determination of an optimal transmission network topology from the system point of view becomes very complicated. In the first stage of optimizing the connections for the entire offshore region, both the transmission technology and network topology need to be determined in parallel.

In finding the optimal network topology for an offshore wind region, OWPPs may be clustered together potentially reducing the required number of OSSs as well as shore connections. Combining, geographically disparate OWPPs makes for a more diverse generation profile which can have a positive effect on the overall system capacity factor and the sizing of equipment [9]. An important consideration in grouping multiple OWPPs on few OSSs is to understand the maximum feasible size of an OSS. As offshore platforms within the oil and gas industry can be an entire order of magnitude larger than those required for OWPPs, the maximum feasible OSS is not limited technologically but rather by what is economically viable [10]. What is economic is a function of local conditions such as available ports, vessels, ease of logistics and sea bed conditions. As a rule of thumb, OSS up to 900 MW are already in wide operation so only beyond this point is a more detailed economic analysis likely required [11].

Finding the optimal topology proves to be the most significant step in reducing the cost and weight of MV and HV equipment. The optimal topology dictates the location, technology, number and ratings of OSSs, cables, transformers and converters. Once the topology is established, only minimal improvements on the selection of individual components can be made. As such, of the 5 stage methodology followed within this report and described by Fig. 3, the first 4 stages involve ensuring that the obtained topology is optimal whereas the last stage focuses on the optimization of the specific equipment for a given topology.

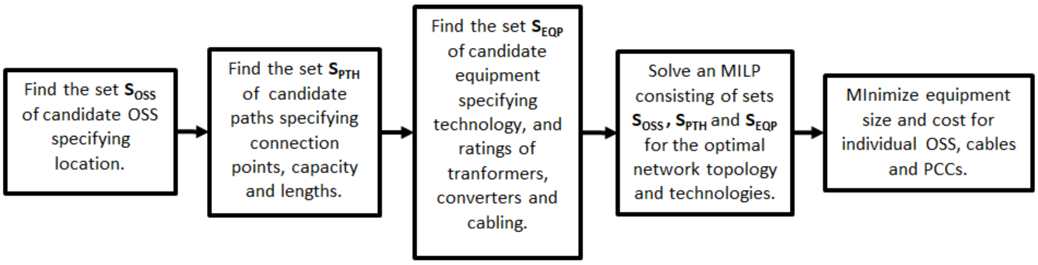

Figure 3: Cost and weight reduction methodology

The first stage involves finding the set of all possible locations an OSS may be constructed. The location an OSS may be constructed is dictated by the possible interconnections between OWPPs. The second stage is finding the set of paths that link the OWPPs and the possible locations of the OSSs. Stage 3 defines specific technology and equipment ratings for the OSSs and paths defined previously. The fourth stage finds the optimal topology of the defined candidate equipment via efficient mathematical methods. The result of stage 4 is the system topology with locations of OSSs defined, transformers or converters sized and ratings of interconnects and shore connections established. The final stage performs a final optimization on individual pieces of equipment established in stage 4.

The remainder of this report is structured as follows. Section 2 describes in detail the methodology employed to obtain the optimal transmission topology, stages 1 to 4 of Fig. 3. First, the intended domain of applicability is defined, then the modelling assumptions for the offshore zone are discussed. The section is concluded by presenting a simple step by step optimization of a 3 OWPPs offshore zone. Section 3 follows, highlighting areas where cost and weight can be reduced for individual pieces of equipment. Finally, conclusions extracted close out the report.

2 OWPP Topology Optimization for Cost Reduction

2.1 Intended Zone of Applicability

The electrical system of OWPPs consists of a medium voltage (MV) and a high voltage (HV) network. The MV network collects and centralizes power generated by individual turbines. The MV network is on the scale of the individual OWPP and is typically not used for shore connections, with the exception of instances where the distance to the point of common coupling (Point of Common Coupling (PCC)) is less than about 15 km [12]. MV offshore networks have traditionally been realized in ac technology and operated at 33 kV. Recent advancements towards higher turbine generator voltage levels mean that 66 kV is now also being deployed as the collector grid voltage [13]. In the literature, dc MV networks are also studied [14]. As MVDC grids have still not been used in any real life offshore application, they are not included within the scope of this report.

The HV network provides bulk power transmission to shore. This can be achieved with either HVAC or HVDC technology. Independent of the choice of technology, it has been common practise for transmission systems to be designed individually for different OWPPs [15]. This has been the case as individual concessions were auctioned off to developers who had little incentive, or ability to cluster with neighbouring concessions. One exception to this is the DolWin3 HVDC substation in Germany, where the HVDC connection serves for two OWPP clusters, namely the Merkur and the Borkum Riffgrund 2 wind farms. As the offshore industry matures however, there has been a realization that substantial savings and increased reliability can be gained if the entire offshore wind zone is treated as a single optimization domain prior to the development of individual concessions [16]. New project proposals like Elia's Modular Offshore grid 2 (MOG2) in the Belgium North Sea are counting on this approach to provide cost reductions [17]. As such, the methodology discussed here within, defines the HV network as not simply point to point transmission for individual OWPPs but as a network used to interconnect and cluster groups of OWPPs, connecting an entire wind region as economically as possible to a or multiple PCCs.

2.2 Modelling an Offshore Wind Zone

Finding the optimal transmission system topology of an offshore wind zone is a problem of considerable complexity. The solution defines the transmission technology or technologies, the number, ratings and locations of transformer or converter stations and the number and ratings of cables between OSSs as well as from OSSs to shore.

As with much in the offshore wind industry, the Offshore wind Zone Topology Problem (OZTP) is still in it's early stages of development. With this being said, the problem shares much in common with the very well studied Transmission Network Expansion Problem (TNEP) [15]. It is therefore important to understand the similarities and the differences between these two problems. In both cases the goal is to find an addition to the electrical network which satisfy grid constraints and circuit physics and whose sum of Capital Expenditure (CAPEX) and Operating Expenditure (OPEX) is minimized. Furthermore, both problems deal with uncertainty of inputs, especially with long planning horizons.

The problems do differ, however, in one very important manner. In TNEPs much of the network is existing and the goal is to find the optimal grid reinforcements (brown field approach). As such, complexity is derived mostly from the size of the network being considered. In contrast, the considered network in OZTPs is much smaller and the complexity is derived from the fact that the entire network is an unknown [15] (green field approach). In OZTP computational complexity stems from large numbers of non-continuous decision variables, representing investment decisions, rather than the calculation of the network constraints and circuit physics. For example, a feasible solution to a medium sized OZTP may consist of only a few buses (OSSs) and half a dozen transmission lines, on which power flow analysis by hand would be possible. Comparing this to TNEPs which can have buses and transmission lines numbering many orders of magnitude higher and requiring powerful computers to calculate power flow. This observation leads to the approach presented in sections 2.4 and 2.5 where an optimization method for the placement of individual OSSs and submarine connections is presented.

Using this understanding and the formulation of the standard TNEP as a starting point a model can be developed. Four basic model definitions divided into two knowns and two unknowns are introduced. The known values are the OWPPs and PCCs. The unknown values are the location and rating of the candidate buses (OSSs), and the connection topology and ratings of the candidate branches (cables).

A OWPP is modelled as a circular area centered around a OWPP geographic centre. The area is given by:

$$OWPP_{area} = \frac{OWPP_{MW}}{\rho_{cap}} \tag{1}$$

where $OWPP_{MW}$ is the power rating of the particular OWPP and ρ_{cap} is the capacity density defined as the ratio of theoretical maximum power which can be harvested in an offshore wind region to the ground area of that particular region. For example, the capacity density of the North Sea is approximately $6\,\mathrm{MW/km^2}$ [18]. An OWPP can only be directly connected to the MV network.

A PCC has both a geographic location and a connection voltage level. In the simplest scenario presented here, a PCC is modelled as an infinite bus. Note that in reality the power in-feed from offshore wind farm clusters might need to be distributed among several PCCs, considering the state of the onshore network.

A candidate OSS is a possible location for an OSS within the network. Candidate OSS may house a transformer or a converter or they may simply act as a collector or compensation platform. A candidate line is a possible transmission line within the network. Candidate lines come in several forms: an MVAC line from the OWPP to an OSS or PCC, an HVAC line connecting two OSSs or an HVAC/HVDC line connecting an OSS and a PCC. Meshed HVDC grids have not yet been considered in this formulation. All possible candidate connections are summarized in Fig. 4.

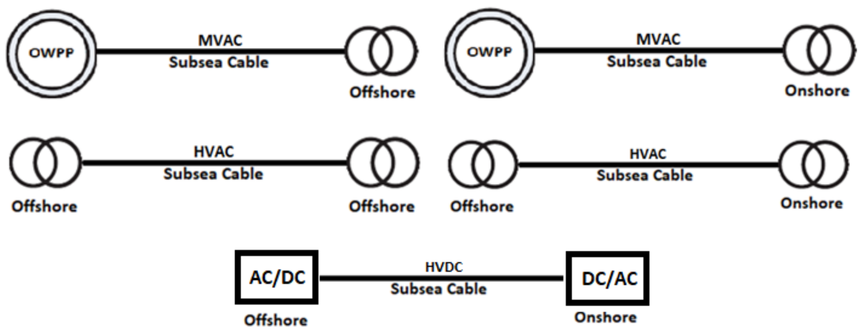

Figure 4: Summary of possible candidate lines

2.3 Economics of Offshore Equipment

For the sake of brevity, the cost functions and full methodology used in the rating of candidate equipment will not be described here in detail. However, for convenience a summary of cost functions is provided in Appendix A and for readers interested in further details the authors refer them to [9] and [7]. Rather, the intent of this section is to briefly highlight the impact of wind variability on the calculation of equipment ratings.

Wind generation profiles such as the one shown in Fig. 5 are utilized in calculating equipment ratings, losses and EENS. It is widely understood,

Table 1: CF and LLF for diverse and non-diverse wind profile.

	Diverse	Non-diverse
CF	0.4	0.4
LLF	0.23	0.29

that the capacity factor Capacity Factor (CF) of a generation profile has an influence on equipment rating as it is representative of how much time the OWPP will operate at full capacity. The CF is defined as,

$$CF = \sum_{n=1}^{THH} \left(\frac{Load_n}{PeakLoad}\right)/THH \tag{2}$$

where THH is the number of half hour periods within a year [19].

The Load Loss Factor (LLF) (3) is a measure of the average losses vs the peak losses, defined as,

$$LLF = \sum_{n=1}^{THH} \left(\frac{(Load_n)^2}{(PeakLoad)^2}\right)/THH \tag{3}$$

and is utilized in calculating system Route Loss Costs (RLCs) and Terminal Loss Costs (TLCs) [9], [19]. The higher the LLF, the higher the average I^2R losses within the system. A property of a wind generation profile is it's diversity of generation. This is the tendency to spend more or less times at the extremes of generation, i.e. 0 and 100%. Diversity increases with geographic and temporal variations in the generating region, as turbines will tend to vary more in power output with relation to each other. The LLF can vary with the diversity of wind profile even while the CF remains constant as table 1 demonstrates for the example profile of Fig. 5. Despite the CF being the same for both profiles, the LLF is higher in the non-diverse case. As such, the optimal rating of equipment is not only affected by what the regionally obtainable CF is but also by the temporal and geographical diversity of the OWPP. Within this work, to account for these effects, the CorWind software is utilized to generate realistic, regionally specific wind profiles. CorWind generates a wind time series through a combination of meteorological reanalysis techniques and stochastic simulations. For further details on CorWind please refer to [20].

2.3.1 Candidate Cable Selection

Undersizing an HVAC export cable has been shown to be economic in certain cases [7]. This is caused by the limited number of available step sizes in HVAC

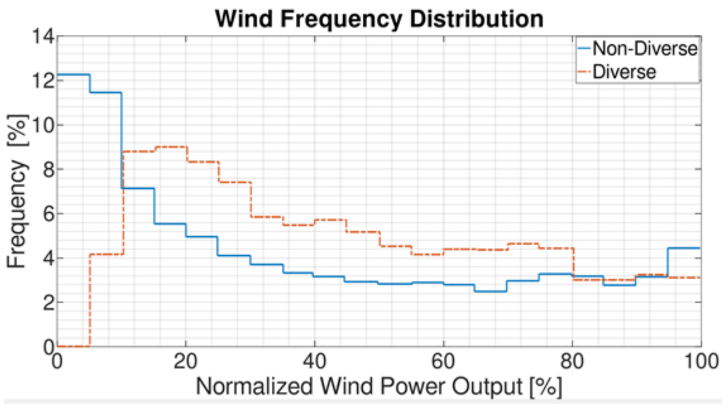

Figure 5: Diverse vs non-diverse wind generation profiles. [9]

cables. This is best understood by examining the cost breakdown presented in Table 2 of HVAC transmission options for an 800 MW OWPP, located 90 km offshore. Option 1 presents undersized export cables with a total capacity of 678 MW, significantly less than the 800 MW OWPP capacity. Still, the lifetime cost of this configuration is less than that of the next available 220 kV cable size presented as option 2. In option 1 it is lower RLCs and Route Construction Costs (RCCs) that more than compensate for the compromise of high EENS from power curtailment. In option 3, increased capacity is obtained via system voltage. Again, however, savings in EENS cannot be justified as the extra cost of RCC results in a net increase. Here it should be noted that such an undersizing of cables will result in a more complicated wind farm controller to restrict the power injection from the wind farms. It also needs to be noted that if wind farms are clustered, the curtailment of access power might result in a conflict of interest between different wind farm owners.

2.3.2 Candidate Transformer Selection

As cables are the largest percentage of transmission system cost it is a logical choice to size transformers based on cable capacity and not on the capacity of the OWPP. Furthermore, the gain in reliability from connecting at least 2 transformers in parallel justifies the increased weight and cost of the OSS [9]. This can be observed by comparing options 1 and 4 of Table 2. The effect on system cost is apparent. A single 800 MW transformer reduces the Offshore Plant and Platform Cost (OPPC) but the increase in EENS out weighs the cost savings. Therefore, the initial investment with two parallel transformers in option 1 is economically the most viable one, from a central

Table 2: Comparative Cost Breakdown of 800 MW HVAC transmission options at 90 km.

Voltage (transformer)	Cable (Capacity)	Total Cost [M€]	OPPC (OPC) [M€]	RCC (QC) [M€]	RLC (TLC) [M€]	EENS (CM) [M€]
220 kV (2-500 MW)	2-1000 mm^2 (678 MW)	339.4	56 (4)	180 (10.9)	27 (16.1)	41.7 (3.7)
220 kV (2-500 MW)	3-500 mm^2 (789 MW)	357.2	56 (4)	220 (12.5)	32.6 (16.1)	12.1 (3.9)
400 kV (2-500 MW)	2-800 mm^2 (1052 MW)	378.8	56 (4)	252 (26)	9.5 (16.2)	12.1 (3.9)
220 kV (1-800 MW)	2-1000 mm^2 (678 MW)	356.2	37.9 (4)	180 (10.9)	27 (16.1)	78.4 (2)

*OPPC: Offshore Plant and Platform Cost. OPC: Onshore Plant Cost. QC: Compensation Cost. CM: Corrective Maintenance Cost.

planner perspective.

2.4 Optimal locating of candidate equipment

The next stage in modelling the offshore region is to determine the optimal location of the candidate OSSs and cables. To demonstrate the optimization process, an example offshore wind region consisting of 3 250 MW OWPPs is used. Fig. 6 shows the region as well as some possible connection scenarios. The OWPPs are labelled A to C, with A being the closest to the PCC and C the furthest. The inner of the 2 concentric circles around each OWPP outlines the OSS area as specified by (1). A capacity density of 6 MW/km^2 is assumed resulting in OWPPs of 41.6 km^2. OSSs are shown as green diamonds, HV connection paths are in black and MV connection paths in red. For this example, a 33 kV MV network is used.

The first step in placing candidate OSS is to make direct connections from each OWPPs to the PCC. These connections are shown on the left side of Fig. 6. The connection paths are made using the shortest possible route and MV cable length is minimized. If a direct MV connection to shore is cheaper than the equivalent MV/HV system, the MV connection is substituted. Next, the location of OSSs for MV connections are calculated. To do this, the break even distance with an HV line of equivalent capacity, including the cost of a platform and transformation, is calculated. This creates an arc of maximum MV range surrounding each OWPP. The outer concentric circles of Fig. 6 show these ranges. An OSS is placed within any overlapping MV feasibility range such as those of OWPPs C and B (Fig. 6 - center).

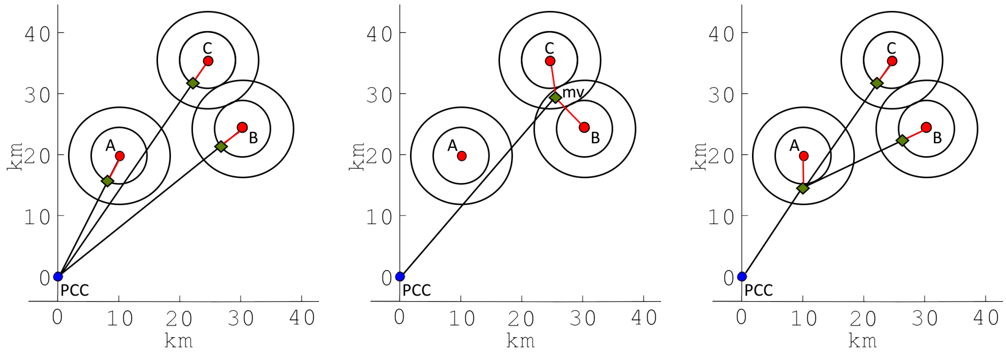

Figure 6: OSS placement for Direct, MV and C&B-A connection.

Calculating the exact location of the MV OSS within these overlapping ranges is done via the minimization of the non-linear system of equations described by (4) to (6), where S is the set of coordinates describing the positions of the OWPPs and PCC being connected. (4) calculates the net length of all paths required to connect the 2 OWPPs and the PCC to a point (x_m,y_m). (5) describes the areas of maximum MV range around each OWPP where R_{mv} is the radius of the circle. The centre of Fig. 6 shows the resulting location of the MV OSS and the paths for the candidate lines.

$$f(x, y) = \sum_{\forall p \in S} \sqrt{(p_x - x)^2 + (p_y - y)^2} \tag{4}$$

$$\left.\begin{array}{l} g(x, y) = (x - p_x)^2 + (y - p_y)^2 \\ g(x_m, y_m) \leq R_{mv}^2 \end{array}\right\} \forall p \in S \setminus \{PCC\} \tag{5}$$

$$\nabla f(x_m, y_m) = \lambda \nabla g(x_m, y_m) \tag{6}$$

After the placement of the candidate OSSs for MV connections, a similar operation for candidate HV OSSs and paths can be performed. The first step in this process is described by the algorithm shown in Fig. 7. The output of the algorithm is all the combinations of points dictating the positions of candidate HV OSSs. These combinations for the example offshore zone are summarized in table 3. In the table, an "→" indicates connected to, an "&" indicates an additional incoming connection and brackets indicate priority of the operation. For example, the entry C&B→A should be understood as

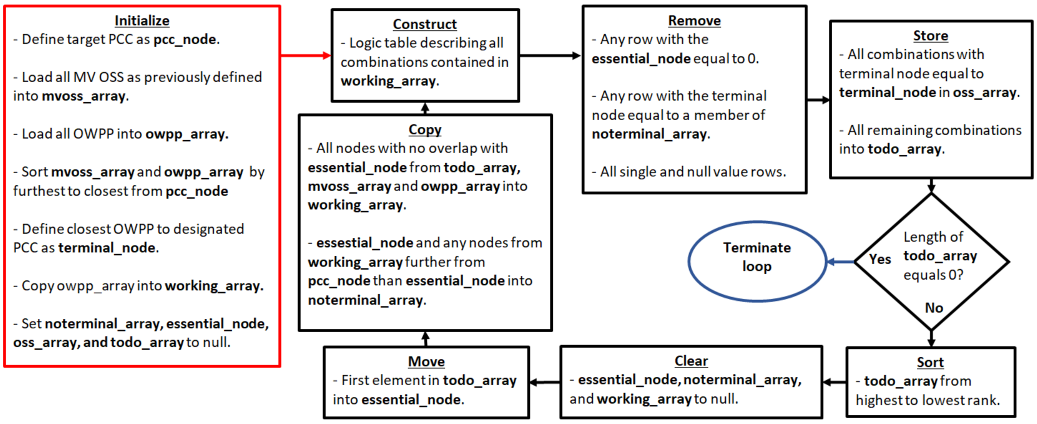

Figure 7: Candidate OSS selection algorithm.

Level 1	(x,y)	Level 2	(x,y)
mv	(27.49,30.02)	mv→A	(9.45,16.16)
C→B	(25.05,25.03)	(C→B)→A	(9.75,15.98)
C→A	(8.96,16.44)		
B→A	(10.03,15.80)		
C&B→A	(10.25,15.66)		

Table 3: Output of candidate OSS algorithm and their locations.

connections from OWPPs C and B connect to OWPP A on an OSS near A. This connection is shown in the right side of Fig.6. The entry (C→B)→A, on the other hand, should be understood as a connection from OWPP C is made to OWPP B on an OSS near B. The OSS near B is then connected to OWPP A via a second OSS near A. This connection is shown in the left of Fig. 8. This type of connection demonstrates a composite calculation, which requires the location of OSS (C→B) to be known in advance. As such positions of OSS specified in the table must be solved from left to right, solving an entire column before moving to the next. This property of the formulation has the benefit that for large problems a decomposition into smaller problems is quite simple. Each column of Table 8 can be solved independently without loss of optimality. Viewing the left side of Fig. 8 demonstrates how this division can be implemented. The connection (C→B)→PCC from the first column of the table and ((C→B)→A)→PCC from the second column are parallel paths of the same capacity therefore would not both form part of the optimal topology.

Calculating the precise positions of the OSSs shown in Table 3 is done in a similar manner to the MV OSSs by solving a non-linear system of equations.

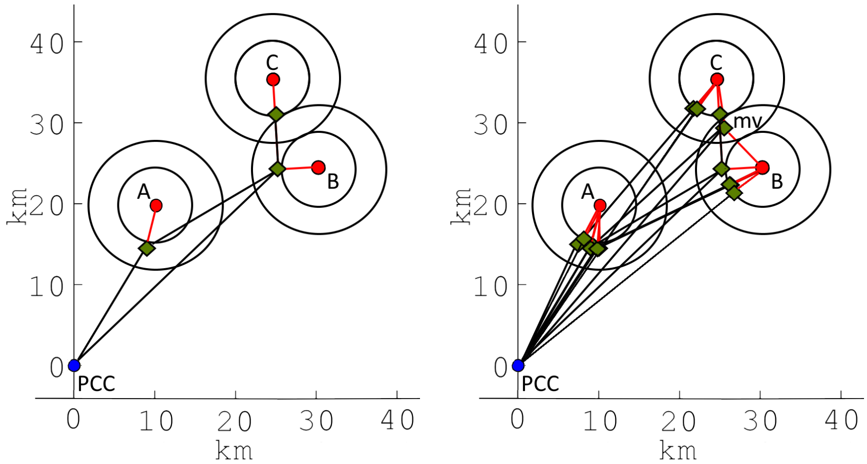

Figure 8: (C-B)-A connection (left), all candidate OSS (right).

(4) and (6) remain unchanged, however, (7) is substituted with (5). In (7), R_{PCC} is the straight line distance from the nearest OWPP being connected and R_{OWPP} is the radius of the OWPP itself. The solution to the system of equations is therefore the minimal length paths required for a connection sitting on the circle of radius $R_{PCC} - R_{OWPP}$ centered around the PCC. The network with all candidates, consisting of 12 OSSs, 16 MV paths and 17 HV paths is shown in the right of Fig. 8. In the next section we will calculate cable, transformer and converter ratings for the candidate OSSs and paths.

$$\left.\begin{aligned} g(x,y) &= (x - x_{pcc})^2 + (y - y_{pcc})^2 \\ g(x_m, y_m) &= (R_{PCC} - R_{OWPP})^2 \end{aligned}\right\} for \min_{p \in A} \|\mathbf{p}, \mathbf{PCC}\| \qquad (7)$$
$$where\ A = S \setminus \{PCC\}$$

2.5 Determination of candidate equipment ratings

In the process of adding the candidate OSSs, the candidate paths also resulted. Each candidate path has an associated length and capacity. Using these 2 values the ratings of candidate cables, transformers and converters are calculated. A detailed description of the cost functions have been published in [7] but for the sake of ease and completeness they are also summarized in appendix A. The ratings and chosen technology for the candidates is a result of choosing the most economic option.

This process applied for the direct OWPPs to PCC connection candidates shown on the left side of Fig. 6, results in each requiring a length of MV cable connecting to an OSS housing a transformer and then a length of HV cable

Equipment	Rating	Length	Cost
33 kV Cable	6-800 mm^2	0.],5 km	3.733 M€
OSS + 33/220 kV			
Transformers	2-130MVA		32.387 M€
220 kV Cable	1-400 mm^2	35.41 km	37.816 M€
		Total	73.936 M€

Table 4: Choice of equipment for direct OWPP B to PCC connection.

spanning the remaining distance to the PCC, all of which must sustain a capacity of 250 MW. To provide a concrete example, the equipment selected and cost for the connection from OWPP B is summarized in table 4. For all candidate connections we can again refer to table 3. As with the positional calculations the table should be processed from left to right.

2.6 Solving for the Optimal Topology

Having found the candidate OSSs and lines the problem has been formulated in a similar manner to a TNEP with the exception that only the candidate grid is considered. The objective of the optimization is to find the lowest cost topology that satisfies power flow constraints and equipment limits. For the representation of the power flow equations and the calculation of losses, there are a wide range of formulations available. One one hand, the exact nonlinear nonconvex 'AC' formulation considers both active and reactive power whereas the linearized 'DC' power flow approximation considers only active power. In the literature there are formulations which attempt to balance accuracy of solution and computational requirements by partially modelling the reactive power using linearizations or convex relaxations [21].

Although 'AC' power flow formulation provides the most accurate solution, problems can quickly become unsolvable due to the non-convex nature of the formulation. Therefore, for large networks a 'DC' power flow formulation is frequently employed [22]. For TNEP under normal conditions, 'DC' power flow provides a reasonably accurate approximation of full 'AC' power flow [23]. As the OZTP is formulated similarly to a TNEP it is likely that the 'DC' power flow is sufficient, however, as submarine AC cables suffer from high capacitance compared to overhead lines, the 'DC' approximation must be used with caution [24]. Furthermore, as noted previously, the computational complexity of OZTP is mostly derived from the high number of binary decision variables rather than power flow. It is possible that by introducing an additional constraint to the optimization problem in the form of an easily calculated objective function upper bound, 'AC' power flow could be feasible

Portion	Equipment	Rating	Length	Cost
C→(C→A)	33 kV Cable	6-800 mm^2	0.5 km	3.733 M€
C→(C→A)	OSS + 33/220 kV			
	Transformers	2-130MVA		32.387 M€
C→(C→A)	220 kV Cable	1-400 mm^2	20.98 km	22.637 M€
A→(C→A)	33 kV Cable	6-800 mm^2	0.569 km	4.0594 M€
A→(C→A)	OSS + 33/220 kV			
	Transformers	2-130MVA		32.387 M€
(C→A)→PCC	220 kV Cable	2-400 mm^2	18.723 km	38.872 M€
			Total	134.075 M€

Table 5: Choice of equipment for C→A connection.

even on large OZTP problems. This requires further investigation and it is the intention of the authors to do so during future work.

Utilizing linear 'DC' power flow allows the OZTP to be solved as a Mixed Integer Linear Program (MILP). This permits the use of efficient algorithms such as the simplex, the branch and bound and branch and cut algorithms. Applying this method to the example problem developed previously gives the optimal topology shown in Fig. 9. The chosen equipment and costs are displayed in tables 4 and 5.

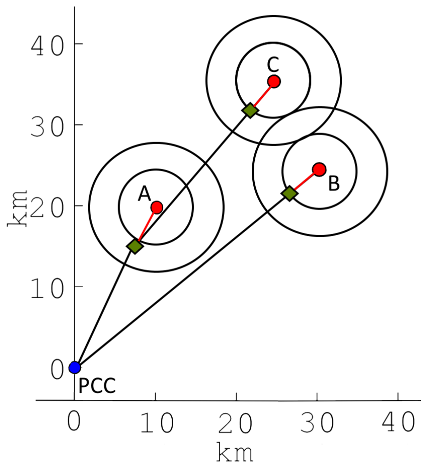

Figure 9: Optimal layout for example Offshore zone.

3 System Cost and Weight Reduction

3.1 HVAC

3.1.1 Transformers

Although the size and number of transformers has been set during topology optimization, the dimensions and mass of each transformer can further be optimized to achieve a trade-off between weight and the transformer losses. The load and no load losses of a transformer can be approximated by (8) and (9), respectively. In (8), N is the number of windings, ρ_{CU} is the resistivity of copper at the operting temperature (75^{o}C), λ_i is the winding fill factor of copper, R_i is it's radius, t_i it's thickness, h_i it's height, α_i the ratio of primary to secondary heights, κ a stray loss estimating factor and Z the short circuit impedance. In (9), M_C is the mass of the core, f_b is the building factor and f(B,H) is the B-H curve of the core material. Both f_b and f(B,H) are properties of the technology and manufacturing technique, they must be provided by the manufacturer. M_C can be further broken down into a sum of component parts written in terms of dimensional volumes and material densities. (8) and (9) provide a relationship between the mass and volume of a transformer and the losses allowing for a cost optimization to be performed on the offshore platform, with the objective being to minimize net cost incurred due to transformer and platform construction and electrical losses over its life time. [25] has demonstrated that (8) and (9) can be effectively formulated as a geometric optimization problem and therefore transformed into a convex problem.

$$P_{ll} = \sum_{i}^{N} 2\pi\rho_{CU}\lambda_i R_i t_i \alpha_i h_i (1 + \kappa Z) \tag{8}$$

$$P_{nll} = M_C \cdot f_b \cdot f(B, H) \tag{9}$$

3.1.2 Cables

The export cable of an OWPP makes up the largest cost single component in an AC offshore transmission system as shown in Fig. 1. As such, cable cost reduction can have a large overall impact on the economics of the transmission system. Traditionally cables are sized considering 100% continuous loading as in IEC-60287-1. Rating in this manner for OWPP connections is not cost effective as capacity factors rarely climb above 50% and current varies with wind conditions. IEC-60853-2 provides an extension allowing for the calculation of cable temperature due to discretely varying load current.

The standard is limited, however, to pre-defined loading patterns. To overcome this limitation, 3 types of models are typically employed: the Finite Element Method (FEM), the step response and the Thermal Electric Equivalent (TEE). Using a TEE model [26] demonstrated that a reduction of cable cross section is possible without affecting lifetime.

The analysis in [26] only considered continuous cross sections of cable. In industry, however, it is not uncommon to divide the length of the cable into shorter sections each with a different cross section. The export cable, including on shore sections, for the Gemini OWPP, for example, consists of 11 sections utilizing 5 different cross sections and both aluminum and copper conductors. It is the belief of the authors that further cost savings on the export cables are possible by considering multiple sections and optimizing cable cross sections for each part. In doing so the limitations imposed by the finite step sizes in cable cross section available may be overcome and a near continuous range of cable capacities obtained.

3.2 Converters

For OWPPs, power electronics converters are essential components in wind turbines and offshore HVDC substations. The converters used in OWPPs are MV and HV converters. As discussed above, the costs of building offshore substructures are expensive, so the size and volume of converters in OWPPs should be minimized.

As an emerging technology, SiC devices have been regarded as a future trend for power electronics converters. Comparing to traditional Si devices, SiC devices feature faster switching speed, higher blocking voltage and higher operating temperature [27]. Faster switching speed allows the converter to operate at higher switching frequency with high efficiency, which can reduce the size and weight of the converters. Higher blocking voltage allows the manufacturing of devices with high voltage ratings with the same number of switching devices, reducing weight and cost. Devices with high voltage ratings will be suitable for the application of MV and HV power electronics converters such as OWPPs. Therefore, SiC devices can be considered as a potential method to reduce the converter volume and weight, in other words, to increase the power density.

The converter weight in OWPPs can be reduced from three aspects by using SiC devices: reduced number of passive components, reduced number of heat sinks and reduced number of submodules of multi-level converters.

SiC MOSFETs are able to switch much faster than Si IGBTs. The switching losses can be significantly reduced due to fast switching speed. As shown in Fig. 11 [29], the turn-off dv/dt of a 10 kV SiC MOSFET can be 12 times

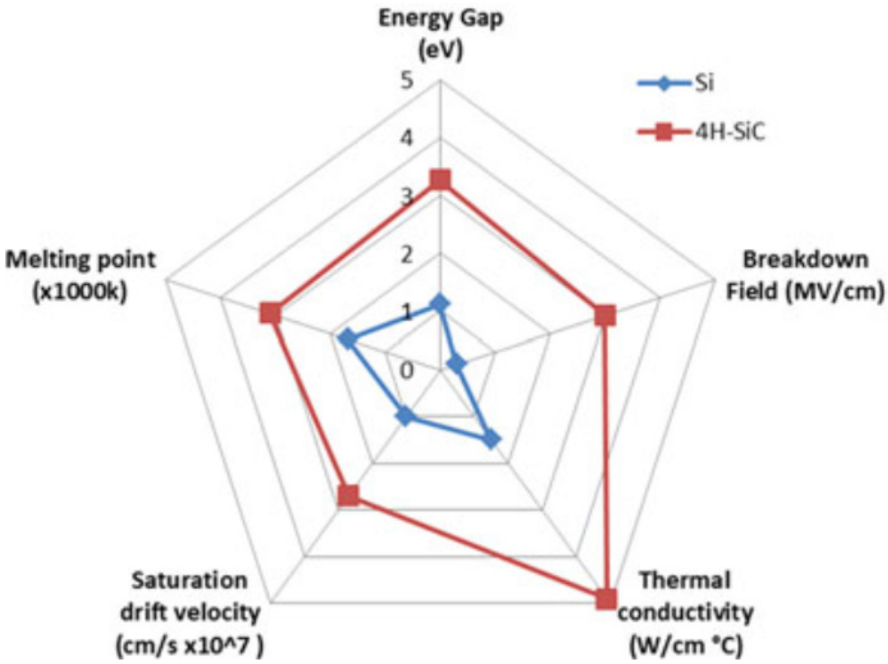

Figure 10: Comparison between Si and SiC materials [28].

faster than a 6.5 kV Si IGBT, resulting in 28 times of switching losses reduction. This allows the converter to operate at higher switching frequency with high efficiency. In power electronics converters, there are many passive components such as filter inductors, filter capacitors and high frequency transformers. For example, L filters or LCL filters are commonly used in grid-connected AC/DC converters to filter out the switching ripples [30]. The parameters of the filter components are related to the switching frequency. The size of the filter components can be reduced significantly when the switching frequency is increased. For isolated DC/DC converters, the size of the high-frequency transformer can also be reduced significantly with the increase of switching frequency as shown in Fig. 12.

Semiconductor devices will generate power losses including switching losses and conduction losses, eventually increasing the device temperature. The device temperature should be maintained within its allowable temperature range, and as such thermal management of power electronics converters should be carefully designed according to the device characteristics. Mostly, heat sinks or water cooling systems are used to dissipate the heat from semiconductor devices. Comparing to Si IGBTs, the SiC MOSFETs have better thermal conductivity and allow for a higher operating temperature. The junction temperature of Si IGBT has an upper limit of 175 °C, while the

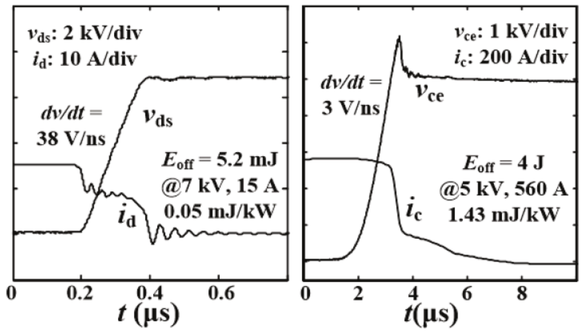

(a) 10 kV/20 A SiC MOSFET (b) 6.5 kV/600 A Si IGBT

Figure 11: Turn-off waveforms of a 10 kV SiC MOSFET and a 6.5 kV Si IGBT [29].

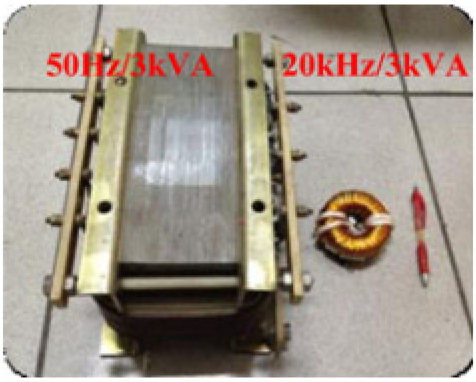

Figure 12: Size comparison between a 50 Hz/3 kVA trnasformer and a 20 kHz/3 kVA transformer [31].

junction temperature of SiC MOSFETs can go beyond 400 °C [32]. Better thermal conductivity allows the heat to dissipate more easily. Higher operating temperatures allow the working temperature of the SiC devices to be higher than Si IGBTs, which can reduce the requirement of heat sinks. These two advantages allow reduced heat sinks or other thermal management equipment in power electronics converters. In [33], an automotive inverter is built based on SiC JFET for 120 °C ambient temperature with air cooling system, while the water cooling system has to be used if the inverter is built based on Si IGBTs.

SiC devices can achieve higher blocking voltage than Si devices. The maximum voltage rating of Si IGBT is 6.5 kV, while 10 kV SiC MOSFETs and 15 kV SiC IGBTs can be achieved. A 10 kV SiC MOSFET has been tested and modelled in [34]. In [35], a three-phase solid-state transformer is developed based on 15 kV SiC IGBTs and 10 kV MOSFETs. In MV and HV applications, multilevel converters are usually used, which requires many semiconductor devices and submodules to withstand the high voltage due to the limited voltage rating of a single device. By using high voltage SiC MOSFETs or IGBTs, the required number of devices and submodules can be reduced, so a more compact converter can be built. In [36], a two-level three-phase inverter is designed based on 10 kV SiC MOSFETs for MV motor drives with a 6 kV DC-link. The power density can achieve 2.5 MW/m^3. If Si IGBTs are used in the same application, multi-level topologies should be used due to the limited voltage ratings and power density will be low.

One of the challenges of using SiC devices is the high cost [37]. SiC devices are more expensive than its Si conterparts. However, the price of SiC devices will reduce in the future as the technology matures and mass production is achieved. On the other hand, although SiC devices are more expensive than Si devices, some researchers have discovered that the overall cost of the whole converter system can be reduced by using SiC devices instead of Si devices in some cases. This is because the costs of filter components and heat sinks are reduced and higher efficiency is achieved. Besides, in OWPPs, if the high voltage SiC devices are used, the number of submodules can be reduced so that less components are required. This might also lead to cost reduction but further study needs to be done. Also, the cost analysis of converters versus weight reduction in OWPPs should consider the cost of building the offshore substructures ,which requires a more detailed study from the whole system point of view.

3.3 Onshore HVDC Converter Station Insulation Coordination

The current practise has been to use point to point High Voltage DC (HVDC) connections for large remote offshore wind farms. In the future, many wind farm clusters might be connected to a meshed HVDC grid. In both cases, an onshore HVDC converter station is needed to connect the main HVAC grid. This chapter discusses the cost function in relation to the insulation coordination of an onshore HVDC converter station.

3.3.1 Insulation Coordination Definition

The insulation coordination is the selection of the equipment dielectric strength, in a way it is able to withstand the operating voltage and overvoltages occurring in any expected climatic and environmental condition. The selection is done according to the protective devices.

3.3.2 The Physical Principle

Given an operating voltage, in the case of an onshore HVDC converter station, the insulation coordination greatly depends on the environmental conditions. In fact, the electrostatic field caused by the direct voltage transmission energisation exerts a time-constant attractive force on the pollution particles. As explained in deliverable D1.1, this phenomenon is detrimental to the insulation performance, therefore the dielectric needed for Direct Current (DC) voltage is most of the time greater than for Alternating Current (AC).
However, if the insulation is designed for indoor use, the pollution does not constitute a major challenge, therefore it can have shorter arcing distances for the same operating direct voltage.

3.3.3 The Consequence on the Onshore Station Cost

It follows that choosing to protect the insulation inside a building reduces the cost of insulation. On the other hand, this increases the cost for expanding the building which usually hosts the converter only. It shall be worth to build a larger building to protect the insulation if the following is verified:

$$\Sigma(Cost_{OI}) > \Sigma(Cost_{II}) + Cost_{BE} + Cost_{CC} \tag{10}$$

where OI=Outdoor Insulation, II=Indoor Insulation, BE=Building Expansion, CC=Climate Control
A detailed explanation of the parameters which influence the cost of insulation follows.

The cost of insulation greatly depends on its length, which is generally defined as Arcing Distance (AD). The profile of insulation is not a vertical line, but a convoluted line, designed to increase the surface and the resistance of the conductive layer upon which it can form. The length of the shortest line connecting the two ends of insulation along the insulator surface is called Creepage Distance (CD).
Each millimetre of Creepage Distance (CD) is able to withstand a certain amount of electric stress. This ratio is defined as the Unified Specific Creepage Distance (USCD) in mm/kVt. Therefore, if the operating voltage is known, it is possible to obtain the CD, by multiplying the Unified Specific Creepage Distance (USCD) by the operating voltage (U). Then, the Arcing Distance (AD), which is the final measurement that takes into account the space needed in height, can be obtained by dividing the CD by the Creepage Factor(CF) (11). The CF is the ratio between CD and AD, and it is usually not larger than 4.3.

$$AD = (USCD \cdot U)/CF \tag{11}$$

For the cost analysis, it is necessary to fix CF and U. The creepage factor is usually set to CF=4. Also, the operating voltage of the HVDC link is usually determined in the very early stages of the project and small variations in the rated voltage can be considered via a step-variable including the onshore station.
As such, the main parameter defining the cost related to insulation coordination of the onshore converter station is the USCD. The USCD greatly varies if the insulation is set to be indoor or outdoor. IEC 60071-5:2015 gives the following recommendations:
It should be noted that the cost of insulation cannot be directly associate

Table 6: Insulation Coordination Recommendations

Recommended USCD (mm/kV)	Indoor or Outdoor	Condition
60	Outdoor	Usual
20-30	Indoor	No condensation only
14	Indoor	Clean and controlled

with the USCD, but that it provides a good estimation of the insulation cost. This is true when the operating voltage and the CF are fixed, as discussed above.
The recommended USCDs show that the outdoor placing of insulation causes it to be taller and more expensive in order to counter the pollution flashover

phenomenon. Whereas, the indoor placing allows a shorter and thus cheaper dielectric. In particular, if the indoor environment does not cause condensation on the insulator surfaces, the arcing distance will be half that of the outdoor solution. Moreover, if the environment is clean and controlled, the AD can further be reduced by four times, with respect to the outdoor solution. On the other hand, the cost of the building expansion and the climate control need to be accounted for.
It is important to specify that with increasing severity of the outdoor pollution indoor solution becomes the more economically favourable option. In fact, the calculated USCD by CIGRE 518 would be larger than the recommended 60 mm/kV.

3.3.4 Insulation Cost Quotes

The insulation involved in the discussion is listed through the following Table.

Table 7: Insulation Cost Estimates

Devices	Purpose	Cost by Zibo Taiguang Electric Power Equipment Co.
Post Insulators	Support HV bus bars	1895.7€/2.1m
Arresters	Overvoltage Protection	NA
Reactor Post	Support Smoothing Reactor	1895.7€/2.1m
Tension Insulators	For conductor to reach bus bars	518.2€/5.5m

3.4 Offshore HVDC Converter Station Insulation Coordination

3.4.1 Cost effective Insulation on Platform

The importance of reducing size and weight of the platform directly implies the reduction of its cost before and after installation. The platform size has a large potential of reduction depending on the Insulation Coordination adopted in it.
The converters installed inside the platform need to be insulated from ground potential. Two main options can be adopted: composite insulators and gas insulated gear. The advantage of using composite insulators is their low cost.

However the advantage provided by gas insulated gear's small size is worth the higher cost. In fact, the reduction of the platform size provided by gas insulation allows an overall larger cost cut.
The reason for the insulation size difference is due to the dielectric strength of the insulating medium. The use of composite insulators means the insulating medium is silicone rubber, fibre glass and mostly atmospheric air. The use of gas insulation presumes the use of specific gases like sulfur hexafluoride or trifluoroiodomethane. More common and less harmful gases can be used for insulation, like carbon dioxide, which have inferior dielectric strength properties, but can be as effective as the harmful gases, if rightly pressurized.

3.5 Auxillary Services

3.5.1 SCADA

On OWPP, the hardware components of the Supervisory Control and Data Acquisition (SCADA) system have a low impact on the total weight of the offshore platforms. Usually, The command centre building and the communication room/server is onshore, while Remote Terminal Units (RTUs) and Met mast tower are offshore. The weight of the RTUs can vary between a few kilograms up to 10s of kilograms depending on the number of I/O ports - e.g MODEL 2208 from Unisen and the 500 series from EFACEC. However, the met mast tower is a data collection and transmission floating/fixed beacon (mainly weather data) [38].

The optimal positioning of the RTUs sensors can reduce the total weight and cost of the system [39]. In addition, the measuring technology of the new sensors can reduce the weight, for example, induction based sensors are heavier than optical based ones.

On the other hand, the cost of the SCADA communication infrastructure is the most expensive component and the reduction of number of communication nodes is not always possible. The table below shows the installation cost of two SCADA examples on offshore wind farms:

Table 8: Offshore Wind Farm SCADA system Costs

Project	Cost	Total Capacity
Nysted wind farm [40] 72 turbines, 2.3 MW each	10.5 M€ C_{st}= 160 k€/turbine	165.6 MW
Offshore Design Engineering (ODE) cost model [41]	1.0 M€ C_{st}= 33.3 k€/turbine	108 MW

In [42] it has been claimed that the cost of a SCADA system per 2.3-3.6 MW turbine is 38.3 k€, including the cost of the communication network. Furthermore [43] has calculated the SCADA cost for an offshore wind farm as proportional to the number of wind turbines, and assumed that the cost (C_{st}) of SCADA/Energy Management Systems (EMS) for a single turbine is:

$$34000 \leq C_{st} \leq 75000 \quad [€/\text{turbine}] \tag{12}$$

Therefore, the estimated cost of SCADA/EMS with n_t turbines is:

$$C_{scada} = n_t C_{st} \quad [€] \tag{13}$$

For example, for a 30 turbine (2.3 MW each – total 69 MW), the SCADA installation cost can be between 1.02 M€ and 2.25 M€. In general, a SCADA system shares between 1 to 4 percent of the total cost of an offshore wind power plant.

Despite the SCADA system for wind generation sharing only a small percentage of the total project cost, it is still higher than SCADA systems for other renewable sources such as solar-panel farms [44]. The reason behind that is the number of RTU sensors per turbine tower and the redundant communication system, for example, each turbine needs at least 16 different sensor [39, 45].

4 Conclusions

Within this report a detailed breakdown of the methodology employed to reduce the cost and weight of OSS has been presented. First, a breakdown of offshore costs was analyzed in order to develop a hierarchy of priorities to optimize the offshore transmission system. It was concluded that the most important stage in cost reduction is the establishment of an optimal topology. The optimal topology dictates what technology is most economic, the location and number of OSS, the transmission line interconnections and the number and ratings of all equipment, i.e. converters, transformers and cables.

A detailed description of how the optimal topology is to be found was presented. The major steps involved are to first generate all possible clustering strategies among the analyzed OWPPs under the assumption of a radial solution. During this stage a method for employing Lagrangian optimization was demonstrated in order to optimally position OSSs utilized for clustering. Once all candidate OSSs and connection paths were established, each was assigned an optimal technology and rating considering CAPEX, lifetime losses, Corrective Maintenance (CM) and EENS. The full set of candidate equipment found was then formulated as a green field TNEP and solved under the constraint of linear power flow as a MILP. A simple 3 OWPP example problem was optimized to demonstrate the full step by step process.

In assigning the technology and ratings for equipment, the importance of realistic, regionally specific wind profiles is shown. The effect geographic and temporal diversity has on CF and LLF was discussed and in turn how these properties can effect the choice of equipment. A specific instance where under sizing export cables and paralleling undersized transformers was presented to demonstrate effective equipment sizing methodology.

In structuring the OZTP as a TNEP special considerations must be made to account for the green field vs brown field approach. The aspect that computational complexity in OZTP stems from a high number of binary decision variables rather than a computationally intensive power flow calculation as in a TNEP is important to understand. This observation is a highly influential factor in determining the final formulation of the optimization.

After having successfully found the transmission system topology a second stage of cost reduction strategies related to individual equipment was presented. Potentials for cost reduction in both HVAC and HVDC equipment were presented as well as auxiliary equipment.

A method for reducing the cost of transformers by modelling the variable and fixed losses as functions of the physical mass and volume was introduced. The trade off between cost of increased mass and volume versus system losses can then be optimized via a geometric optimization formulation.

The current sizing methodology of an AC export cable was presented as overly conservative and modelling methods to reduce cable cross section without loss of life were discussed. As the AC export cable has been shown to be the single most costly component in an AC transmission system, this is a very important consideration and was therefore taken a further step by suggesting that the length of the cable be divided into sections which could each individually have an optimal cross section.

A method for reducing the size and weight of power electronics converters by using SiC MOSFETs was introduced. SiC MOSFETs can operate at higher switching frequency with high efficiency. Also, SiC MOSFETs can withstand higher temperature and higher blocking voltage. Therefore, higher power density can be achieved due to smaller filter components, heat sinks and higher voltage ratings of the devices. However, the overall cost should be further analyzed because SiC MOSFETs are more expensive than its Si counterparts.

The Insulation Coordination consequences on cost have been discussed for both the onshore and the offshore apparatus needed to integrate wind power generation into the onshore main grid for consumption of the load centers. For the onshore station it is possible to conclude that the protection of composite insulators inside a building is economically convenient in coastal environments characterised by a high salinity content in air. An alternative solution would be to build the connection to the onshore power system further inland, but an additional investigation is needed to assess the additional cable cost and the consequent overall system cost.

For the offshore station it is possible to conclude that gases like sulfur hexafluoride, trifluoroiodomethane or pressurized gases such as carbon dioxide should be used in instead of composite insulators due to the size, weight and cost reduction of the platform. The higher cost of gas insulated solutions is payed off by the cost reduction of the platform during its manufacturing, transportation, installation and maintenance phases.

Finally, the weight and cost of SCADA devices were discussed. The main offshore weight contribution comes from the communication medium, sensors and actuators (RTUs). It can be concluded that by optimally locating the RTUs, a reduction of the total cost and the overall weight of the offshore SCADA hardware can be achieved.

5 Appendix A - Cost Functions

Table 9: Modeling Assumptions

Variable	Definition	Assumed Value
FC_{hvac}	Fixed cost of HVAC transformer platform	5.6 M€
FC_{hvdc}	Fixed cost of offshore HVDC platform	28 M€
FC_{ofac}	Fixed cost of offshore OFAC station platform	5.6M €
fc_T	Variable cost of HVAC transformer platform	0.0224 €/VA
pc_T	Variable Cost of HVAC offshore plant cost	0.028 €/VA
c_{con}	Variable cost of offshore HVDC converter	0.123 €/VA
Qc_{off}	Unit cost of offshore compensation	0.028 €
Qc_{on}	Unit cost of onshore compensation	0.0168 €/VAR
E_{op}	Cost of energy	56 €/MWh
T_{op}	Total operational hours	365x24x15 hrs
δ	Load Loss Factor	23 %
dc	Cost factor for >1 OSS transformer or converter	0.2
pf	Power factor	1
CF	Capitalization Factor	10
η_{offt},η_{ont}	Efficiency of the offshore/onshore transformer	99.4 %
η_{oni}	Efficiency of the onshore inverter station	98.19 %
η_{offr}	Efficiency of the offshore rectifier station	98.28 %
η_{acac}	Onshore AC/AC converter efficiency	99.12 %

5.1 Capital Expenditure (CAPEX)

5.1.1 Offshore Sub-Station (OSS)

An OSS is modelled as the sum of a variable cost (14), which scales with capacity and a fixed cost (15), representing the float out and erection.

$$OSS_v = [1 + dc \cdot (n_T - 2)] \cdot (fc_T + pc_T) \cdot n_T \cdot S_{ST} \tag{14}$$

$$OSS_f = FC \tag{15}$$

5.1.2 Point of Common Coupling (PCC)

The PCC is modelled as a variable cost related to the required transformer capacity (16).

$$PCC = 0.03327 \cdot S_T^{0.7513} \tag{16}$$

5.1.3 Compensation

The amount of required compensation, Q, to maintain unity power factor is given by (17). Compensation is assumed to be evenly distributed on either side of the cable. The cost of the compensation is calculated via (18). For cables connecting 2 offshore platforms $Qc_{off} = Qc_{on}$.

$$Q = V_n^2 \cdot 2\pi f_n C_{qc} \cdot l_c \cdot n_c \tag{17}$$

$$QC = Qc_{off} \cdot Q_{off} + Qc_{on} \cdot Q_{on} \tag{18}$$

5.1.4 Cable

Cable cost (19) is a function of length, cable type and number of parallel cables. The capacity of a single cable of length l, is given by (20).

$$CBC = n_c \cdot c_{cbl} \cdot l_c \tag{19}$$

$$P_C = \sqrt{S_{cbl}^2 - Q_{on}^2} \tag{20}$$

5.2 Operating Expenditure (OPEX)

5.2.1 OSS Losses

Transformer and cable losses are given by (21) and (22) respectively.

$$TLC = S_T \cdot pf \cdot (1 - \eta) \cdot T_{op} \cdot \delta \cdot E_{op} \tag{21}$$

5.2.2 Cable Losses

$$RLC = \left(\frac{S_T \cdot pf \cdot \eta}{n_c \cdot V_n} \right)^2 \cdot r_c \cdot l_c \cdot n_c \cdot T_{op} \cdot \delta \cdot E_{op} \tag{22}$$

5.2.3 Expected Energy Not Served (EENS)

The calculation of EENS is as follows: If the per unit constrained capacity of system configuration i; $S_{cons,i}$, has a probability of occurring, $P_{cons,i}$, then EENS_i is given by

$$EENS_i = A_{cons,i} \cdot P_{cons,i} \cdot S_{pcc}. \tag{23}$$

Where $A_{cons,i}$ is the area under the input profile curve and above the line y=$S_{cons,i}$ (representative curve shown in fig 13). The EENS of the network is then the sum of all EENS_i over n possible configurations. A Capacity

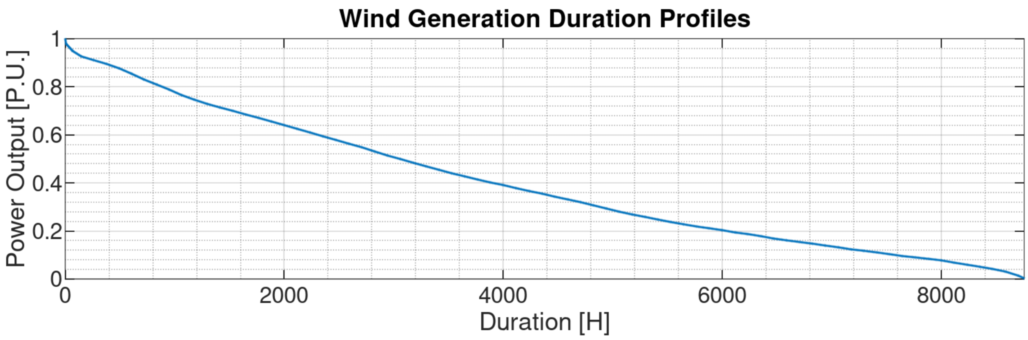

Figure 13: Wind Duration Profiles

Outage Probability Table (COPT) is used when calculating the capacities and probabilities of the n network configurations and is constructed as in 10 using (24) to (27) and table 11. Where FR is Failure Rate, MTTR is Mean Time To Repair and MC is Mean Cost of Repair.

$$A_i = \frac{1}{1 + FR_i \cdot \frac{MTTR_i \cdot 30 \cdot 24}{8760}}, \tag{24}$$

Table 10: Example COPT

State	Capacity ($S_{cons,i}$)	Probability ($P_{cons,i}$)
1	C_i	A_i
0	0	1-A_i

$$C_k =: \begin{cases} C_i + C_j & Series \\ min(C_i, C_j) & Parallel \end{cases} \tag{25}$$

$$P_k = P_i \cdot P_j \tag{26}$$

5.2.4 Corrective Maintenance

Table 11: Reliability Parameters [9]

Equipment	FR [$1/yr$]	MTTR [$months$]	MC [$M€$]
Transformers	0.03	2-onshore 6-offshore	2.75
Converters	0.12	1	0.56
Cables	0.08/100km	2	0.56

$$CM = \left[\frac{n_t \cdot MC_t}{\frac{1}{FR_t} + \frac{MTTR_t}{T}} + \frac{n_c \cdot MC_c}{\frac{1}{FR_c} + \frac{MTTR_c}{T}} + \frac{n_{dc} \cdot MC_{dc}}{\frac{1}{FR_{dc}} + \frac{MTTR_{dc}}{T}} \right] \cdot CF \tag{27}$$

References

[1] Tiago Antunes, Tiago Alexandre dos Reis Antunes, Paulo Jorge da Costa Santos, and Armando José Pinheiro Marques Pires. Limitations of HVAC Offshore Cables in Large Scale Offshore Wind Farm Applications. Technical report.

[2] Morten Holmager, editor. *Offshore Book An introduction to the offshore industry*. Offshore center Denmark.

[3] O. Bolado M. Bollen M. Bradt C. Brooks W. Dilling M. Edds W. J. Hejdak D. Houseman S. Klein F. Li J. Li P. Maibach T. Nicolai J. Patiño S. V. Pasupulati N. Samaan S. Saylors T. Siebert T. Smith M. Starke R. Walling E.H. Camm, M. R. Behnke. Wind power plant substation and collector system redundancy, reliability, and economics. *IEEE PES Wind Plant Collector System Design Working Group*, 2009.

[4] T. Ruddy R. A. Walling. Economic optimization of offshore windfarm substations and collection systems. *GE Energy*, March 2005.

[5] M. Taylor et al. The power to change, solar and wind cost reduction potential to 2025. Technical Report ISBN 978-2-95111-97-4, IRENA, 2016.

[6] Hakan Ergun, Dirk Van Hertem, and Ronnie Belmans. Cost of wind. pages 753–758. Betancourt, U, ENERGYNAUTICS GMBH, 2010.

[7] IEEE PES PowerTech Milano. *Techno-Economic Analysis of HVAC, HVDC and OFAC Offshore Wind Power Connections.*, 2019.

[8] D. Elliott, K. R. W. Bell, S. J. Finney, R. Adapa, C. Brozio, J. Yu, and K. Hussain. A comparison of ac and hvdc options for the connection of offshore wind generation in great britain. *IEEE Transactions on Power Delivery*, 31(2):798–809, April 2016.

[9] Predrag Djapic and Goran Strbac. Cost benefit methodology for optimal design of offshore transmission systems. Technical report, BERR Department for Business Enterprise and Regulatory Reform, July 2008.

[10] Structurae: International Database and Gallery of Structures troll a platform. `https://structurae.net/structures/troll-a-platform`. Accessed: 2019-08-05.

[11] 4C Offshore offshore hvdc converter hvac grid collector database. `https://www.4coffshore.com/transmission/converters.aspx`. Accessed: 2019-08-05.

[12] Josef Schachner. *Power Connections for Offshore Wind Farms Diploma Thesis*. PhD thesis, TU Delft, 2004.

[13] L. Greedy T. Schlemmer. Nl offshore wind farm transmission systems. 66 kv systems for offshore wind farms tennet. Technical Report 74107077-1, TENNET, 2015.

[14] Stefan Lundberg. *Wind Farm Configuration and Energy Efficiency Studies - Series DC versus AC Layouts*. PhD thesis, Department of Energy and Environment Chalmers University of Technology Goteborg, Sweden, 2006.

[15] S. Lumbreras and A. Ramos. Offshore wind farm electrical design: a review. *Wind Energy*, 16(3):459–473, April 2013.

[16] Renewable grid Integration Conference India. *A Techno-Economic MILP Optimization of Multiple Offshore Wind Concessions*, 2019.

[17] ENTSOE project 120 - mog ii: connection of up to 2 gw additional offshore wind belgium. `https://tyndp.entsoe.eu/tyndp2018/projects/projects/120`. Accessed: 2019-08-05.

[18] EU MSP Platform capacity densities of european offshore wind farms. `https://www.msp-platform.eu/practices/capacity-densities-european-offshore-wind-farms`. Accessed: 2019-08-05.

[19] PR Hyland. Guidelines on the calculation and use of loss factors. Technical report, Hyland McQueen Limited, Electricity Authority Te Mano Hiko, February 2013.

[20] Matti Koivisto, Kaushik Das, Feng Guo, Poul SÃ¸rensen, Edgar NuÃ±o, Nicolaos Cutululis, and Petr Maule. Using time series simulation tools for assessing the effects of variable renewable energy generation on power and energy systems. *Wiley Interdisciplinary Reviews: Energy and Environment*, 8(3):e329, 2019.

[21] Hakan Ergun, Jay Dave, Dirk Van Hertem, and Frederik Geth. Optimal power flow for ac/dc grids: Formulation, convex relaxation, linear approximation and implementation. *IEEE Transactions on Power Systems*, 34(4), 2019.

[22] B. Stott, J. Jardim, and O. Alsac. Dc power flow revisited. *IEEE Transactions on Power Systems*, 24(3):1290–1300, Aug 2009.

[23] Carleton Coffrin and Pascal Van Hentenryck. A linear-programming approximation of ac power flows. *INFORMS Journal on Computing*, 26(4):718–734, 2014.

[24] H. Ergun, D. Van Hertem, and R. Belmans. Transmission system topology optimization for large-scale offshore wind integration. *IEEE Transactions on Sustainable Energy*, 3(4):908–917, Oct 2012.

[25] T. Orosz and I. Vajda. Design optimization with geometric programming for core type large power transformers. *De Gruyter open, Electrical, Control and Communication Engineering*, June 2014.

[26] Juan-Andrés Pérez-Rúa, Kaushik Das, and Nicolaos Antonio Cutululis. Lifetime estimation and performance evaluation for offshore wind farms transmission cables. 2019. 15th IET international conference on AC and DC Power Transmission ; Conference date: 05-01-2019 Through 07-01-2019.

[27] Fei Wang, Edward A Jones, and Zheyu Zhang. *Characterization of wide bandgap power semiconductor devices*. Institution of Engineering & Technology, 2018.

[28] J. Millán, P. Godignon, X. Perpiñà, A. Pérez-Tomás, and J. Rebollo. A survey of wide bandgap power semiconductor devices. *IEEE Transactions on Power Electronics*, 29(5):2155–2163, May 2014.

[29] S. Ji, Z. Zhang, and F. Wang. Overview of high voltage sic power semiconductor devices: development and application. *CES Transactions on Electrical Machines and Systems*, 1(3):254–264, Sep. 2017.

[30] S. Acharya, A. Anurag, Y. Prabowo, and S. Bhattacharya. Practical design considerations for mv lcl filter under high dv/dt conditions considering the effects of parasitic elements. In *2018 9th IEEE International Symposium on Power Electronics for Distributed Generation Systems (PEDG)*, pages 1–7, June 2018.

[31] B. Zhao, Q. Song, W. Liu, and Y. Sun. Overview of dual-active-bridge isolated bidirectional dc–dc converter for high-frequency-link power-conversion system. *IEEE Transactions on Power Electronics*, 29(8):4091–4106, Aug 2014.

[32] T. Funaki, J. C. Balda, J. Junghans, A. S. Kashyap, H. A. Mantooth, F. Barlow, T. Kimoto, and T. Hikihara. Power conversion with sic devices at extremely high ambient temperatures. *IEEE Transactions on Power Electronics*, 22(4):1321–1329, July 2007.

[33] B. Wrzecionko, D. Bortis, and J. W. Kolar. A 120 °c ambient temperature forced air-cooled normally-off sic jfet automotive inverter system. *IEEE Transactions on Power Electronics*, 29(5):2345–2358, May 2014.

[34] S. Ji, S. Zheng, F. Wang, and L. M. Tolbert. Temperature-dependent characterization, modeling, and switching speed-limitation analysis of third-generation 10-kv sic mosfet. *IEEE Transactions on Power Electronics*, 33(5):4317–4327, May 2018.

[35] S. Madhusoodhanan, A. Tripathi, D. Patel, K. Mainali, A. Kadavelugu, S. Hazra, S. Bhattacharya, and K. Hatua. Solid-state transformer and mv grid tie applications enabled by 15 kv sic igbts and 10 kv sic mosfets based multilevel converters. *IEEE Transactions on Industry Applications*, 51(4):3343–3360, July 2015.

[36] S. Madhusoodhanan, K. Mainali, A. Tripathi, K. Vechalapu, and S. Bhattacharya. Medium voltage ($\geq$ 2.3 kv) high frequency three-phase two-level converter design and demonstration using 10 kv sic mosfets for high speed motor drive applications. In *2016 IEEE Applied Power Electronics Conference and Exposition (APEC)*, pages 1497–1504, March 2016.

[37] X. She, A. Q. Huang, Ó. Lucía, and B. Ozpineci. Review of silicon carbide power devices and their applications. *IEEE Transactions on Industrial Electronics*, 64(10):8193–8205, Oct 2017.

[38] A. L. Pettener. Scada and communication networks for large scale offshore wind power systems. In *IET Conference on Renewable Power Generation (RPG 2011)*, pages 1–6, Sep. 2011.

[39] Mohamed A. Ahmed and Chul-Hwan Kim. Communication architecture for grid integration of cyber physical wind energy systems. *Applied Sciences*, 7(10), 2017.

[40] G. Gerdes, A. Tiedemann, and S. Zeelenberg. Case study: European offshore wind farms - a survey for the analysis of the experiences and lessons learnt by developers of offshore wind farms. Technical report, Deutsche WindGuard and German Energy Agency (DENA) and University of Groningen, 01/08 2008.

[41] Study of the costs of offshore wind generation. Technical report, Offshore Design Engineering (ODE) Limited, 2007.

[42] C A Morgan, H M Snodin, and N C Scott. Offshore wind economies of scale, engineering resource and load factors. Technical report, Dept of Trade and Industry / Carbon Trust, 2003.

[43] M. Dicorato, G. Forte, M. Pisani, and M. Trovato. Guidelines for assessment of investment cost for offshore wind generation. *Renewable Energy*, 36(8):2043–2051, 2011.

[44] Wireless solar communications technology reduces cost and is easier to maintain, 2016. SunEnergy1 & Duke Energy Renewables.

[45] Mohamed A. Ahmed and Young-Chon Kim. Communication network architectures for smart-wind power farms. *Energies*, 7(6):3900–3921, 2014.

[46] X. Jiang, J. Yuan, L. Shu, Z. Zhang, J. Hu, and F. Mao. Comparison of DC pollution flashover performances of various types of porcelain, glass, and composite insulators. 23(2):1183–1190.

[47] J. M. Seifert, W. Petrusch, and H. Janssen. A comparison of the pollution performance of long rod and disc type HVDC insulators. 14(1):125–129.

[48] L. Bing, Li Licheng, R. Hong, and Li Xiaolin. Study on pollution flashover characteristics of Â±800kv DC composite insulators. In *2007 IEEE Power Engineering Society Conference and Exposition in Africa - PowerAfrica*, pages 1–5.

[49] R Matsuoka, S. Ito, K Tanaka, and K Kondo. Contamination withstand voltage characteristics of polymer insulators. In *10th International Symposium on High Voltage Engineering*. ISH.